Synthesis of Mn^{2+} doped ZnS by a mechanically induced self-sustaining reaction

M. A. Avilés[1], J. M. Córdoba[1,2], M. J. Sayagués[1] and F. J. Gotor[1]

[1]Instituto de Ciencia de Materiales de Sevilla (US-CSIC), 41092 Sevilla, Spain

[2]Departamento de Química Inorgánica, Universidad de Sevilla, 41012 Sevilla, Spain

Abstract

The mechanochemical process denoted as mechanically-induced self-sustaining reaction was successfully applied in obtaining Mn-doped ZnS samples with a Mn content between 0 and 5 mol%. The process consists in milling Zn/Mn/S powder elemental mixtures with the appropriate stoichiometry, which promotes after approximately 80 min the induction of a combustion reaction. The doping level was properly adjusted by controlling the atomic ratio of the starting mixture. A complete characterization of samples was carried out, including X-ray diffraction, high-resolution transmission electron microscopy, selected area electron diffraction, energy dispersive X-ray spectroscopy, Raman spectroscopy, diffuse reflectance UV–Vis spectroscopy and emission and excitation photoluminescence measurements. A wurtzite structure, in which Mn^{2+} replace Zn^{2+}, was obtained with a nanometric character. The photoluminescence of samples showed the characteristic Mn^{2+} ^{4}T$_1$-^{6}A$_1$ emission that was highly dependent on the doping level. The maximum luminescence efficiency through the ZnS excitation was found for a doping value of 1 mol%. The photoluminescence showed virtually no contribution from the host emission, which confirmed that samples were properly doped.

KEYWORDS: Mechanochemistry, Milling, Combustion process, Semiconductor, Optical properties

1. INTRODUCTION

The applications of nontoxic ZnS in some fields, such as solar cells, bioimaging, sensors and optoelectronics, are limited due to the wide-band gap energy (3.6 and 3.8 eV for the zinc blende and wurtzite structures, respectively). Doping is a successful strategy to overcome this limitation since it introduces intermediate-energy levels in the band gap region [1-4]. Therefore, new electronic transitions and de-excitation paths between excited and ground states are possible and allow obtaining multiple wavelength emissions in the visible from a single excitation source [5]. Mn^{2+} is a common doping ion that induces an extra orange luminescence at ~ 580 nm in ZnS under near UV excitation as a result of the strong interaction between the Mn^{2+} d states and the band states of the ZnS host [6]. The excited electrons from the conduction band (or the surface states of ZnS) are transferred to the Mn d levels, through which the radiative de-excitation at ~ 580 nm occurs via the $^4T_1$–$^6A_1$ transition [7]. The percentage of dopant strongly affects the photoluminescence emission of ZnS. At increasing Mn concentrations, the orange luminescence is firstly enhanced, reaching a maximum at a critical dopant concentration, from which luminescence progressively quenches due to recombination processes. However, there is a controversy in the literature about the critical dopant concentration value allowing the maximum luminescence efficiency [8-10], as it is highly dependent on the synthesis method and the final morphology of Mn-doped ZnS.

Mn-doped ZnS is frequently synthesized by low temperature solution-based methods (precipitation, microemulsion, sol–gel, hydrothermal, reverse micelle…) [11-14] or evaporation processes (thermal evaporation, chemical vapor deposition…) [15,16]. These methods have some disadvantageous, such as high chemical complexity, the use of expensive chemical reagents, the need for prolonged reaction time and/or high pressure conditions. Moreover, the Mn^{2+} concentration incorporated in ZnS is sometimes lower

than the Mn^{2+} precursor concentration present during the synthesis procedure [17,18]. Combustion synthesis methods, which use the high exothermic character of a reaction to form the desired product, have also been reported to obtain Mn-doped ZnS [19-24]. These methods are claimed to be direct, simple, cost-effective, time-saving and suitable for large scale production [25]. The reactions involved in these methods are exothermic enough to proceed, once ignited, in a self-sustaining manner, in such a way that the full conversion can be achieved in a short period of time without any additional external energy input.

Combustion synthesis methods differ, among other aspects, in how ignition is induced and the nature of the self-sustained driven reaction. For example, in solution combustion synthesis (SCS), which is carried in an aqueous solution, the heat release during the process comes mainly from the oxidation of an organic fuel and not from the formation reaction of the intended product [19,26]. This contrasts with self-propagating high-temperature synthesis (SHS), a solid state process in which the own formation reaction of the product is the source of the heat release during the process [20-24,27]. Note that ZnS formation from elemental Zn/S mixtures is highly exothermic ($\Delta H_f^0 = -205$ kJ/mol) [28], with an adiabatic temperature (T_{ad}) of 2173 K [21] that fulfills the empirical criterion ($T_{ad} > 1800$ K) [29] for the occurrence of combustion processes. Moreover, it has been shown in the bibliography that it is also possible to ignite a combustion reaction by applying mechanical energy (for example, by ball milling) to highly exothermic reactant mixtures [30]. In these cases, the mechanochemical process that induces a combustion process is referred to as a mechanically induced self-sustaining reaction (MSR). In this sense, ZnS has already been obtained by MSR from Zn/S mixtures [31-34]. Therefore, it would also be possible to synthesize Mn-doped ZnS by this same procedure, since the introduction of small amounts of Mn in the reactant mixture would not change ostensibly the exothermic character of the process.

Few reports can be found in the bibliography dealing with the synthesis of Mn-doped ZnS by ball milling methods [35-38]. In [35] and [36] Mn-doped ZnS samples were obtained by milling Zn, S and Mn powders. The authors did not observe a combustion process and obtained a zinc blende major phase after several hours of milling. Tolia et al [37] synthesized by a mechanochemical method doped sulfide samples from zinc acetate, manganese acetate and sodium sulfide. Finally, Hamaguchi et al [38], starting from commercial microsized ZnS:Mn^{2+}, obtained ZnS:Mn^{2+} nanoparticles by ball milling in a solvent medium. Nevertheless, in this work, a comminution process and not a mechanochemical one was carried out, since no chemical changes were induced during milling, but only a reduction of the particle size. Considering this background, the aim of the present work was to study, first, the ability of the MSR process to obtain Mn-doped ZnS from elemental mixtures and, second, to investigate the structure, microstructure and photoluminescence properties of such-as obtained samples as a function of the doping level.

2. EXPERIMENTAL PROCEDURE

Zinc powder (99% pure, < 325 mesh, Strem Chemicals), sulfur powder (99.5% pure, < 325 mesh, Alfa Aesar), manganese powder (99.3% pure, < 325 mesh, Alfa Aesar) and high-purity argon gas (H$_2$O and O$_2$ < 3 ppm, Linde) were used in this work for the synthesis of Mn-doped ZnS by an MSR process using a planetary ball mill (Micro Mill Pulverisette 7, Fritsch). All of the milling experiments were conducted under an Ar atmosphere (6 bar) using 3 g of Mn/Zn/S elemental mixtures with different Mn doping level (0, 0.5, 1, 1.5, 2, 3, 4 and 5 mol%). Six AISI 420C stainless steel balls (d = 15 mm and m = 13.7 g), a 60 mL tempered steel vial (inner diameter = 45 mm) and a rotational speed of the supporting disk of 400 rpm were employed. The occurrence of an MSR

4

process could be detected during milling, since the vial with a special lid was continuously connected to the gas cylinder by a rotating union (model 1005-163-038, Deublin) and a semi-rigid polyamide tube (Legris), and the Ar pressure was monitored by a pressure transducer (AKS, Danfoss) connected to a paperless recorder (Ecograph T RSG35, Endress + Hauser). At ignition, the heat released by the exothermic reaction of the Mn-doped ZnS formation provokes an instantaneous increase in the total pressure of the system that resulted in the appearance of a sharp peak in the pressure-time record. The critical milling time necessary to induce ignition is called the ignition time (t_{ig}) and depends on the milling conditions. For all samples, milling was stopped 10 min after the detection of ignition in the pressure-time record, which occurred approximately after 80 min of milling (Figure 1).
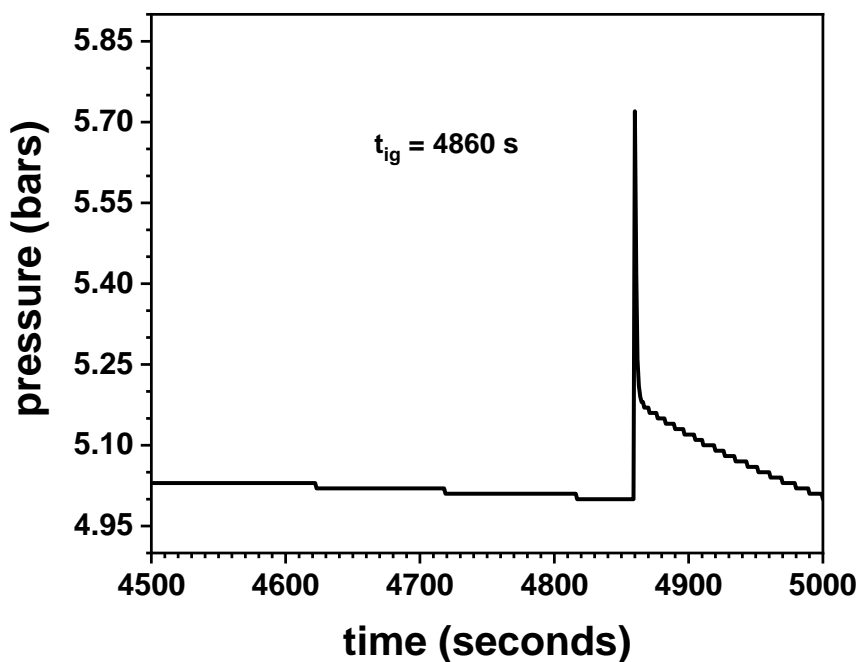

Figure 1. Plot of the pressure-time record during the MSR process corresponding to the formation of Mn (3 mol%)-doped ZnS sample, from which t_{ig} can be properly determined.

XRD patterns of samples were obtained on a X'Pert Pro MPD diffractometer (PANalytical) equipped with a θ/θ goniometer, a graphite-diffracted beam monochromator and a solid-state detector (X'Celerator). The diffraction patterns were

acquired using Cu Kα radiation over a 2θ-range of 10° to 140° with a step size of 0.033° and a counting time of 800 s/step. Silicon powder (Standard Reference Material 640c, NIST) was used for calibration of the diffraction line positions. The quantification of phases detected in the XRD patterns was performed by means of the Rietveld method using the FULLPROF program. Background points, zero point, scale factor, pseudo-Voigt parameters of the peak shape and cell parameters were refined. The following reference diffraction patterns from the PDF-4 + database of the International Centre for Diffraction Data (ICDD) were used as the initial model: ZnS (F-43m, a = b = c = 5.4060 Å; 05-0566) and ZnS (P6$_3$mc, a = b = 3.8210, c = 6.2573 Å; 36-1450). The transmission electron microscopy (TEM) and high resolution (HRTEM) images, electron diffraction patterns (EDP) and energy dispersive X-ray (EDX) spectra, from powder samples dispersed in ethanol and deposited onto a carbon coated copper grid, were taken on a 200 kV JEOL-2100-PLUS microscope equipped with a LaB$_6$ filament (point resolution = 0.25 nm). The HR micrograph analysis, lattice spacing, fast Fourier transform (FFT) and phase interpretation were done with the Gatan Digital Micrograph software (Gatan Inc.) and the Java version of the electron microscope software (JEM).

Raman spectroscopy was performed using a dispersive Horiba Jobin Yvon HR800 confocal Raman Microscope (HORIBA) equipped with a charge-coupled device (CCD) detector at a laser excitation wavelength of 780 nm (red laser). The spectral resolution was 4 cm^{-1}. The laser beam was focused on the powder samples with a confocal objective of 100×. The diffuse reflectance UV–Vis spectroscopy (DRS) was performed using a Cary 300 spectrophotometer from 200 to 800 nm. Band gap (E$_g$) energy was calculated from the corresponding Kubelka–Munk functions, F(R∞), which are proportional to the absorption of radiation, by plotting (F(R∞) × hν)$^{1/2}$ against hν. The emission and excitation photoluminescence spectra (PL and PLE) of samples were measured using a

FLS1000 photoluminescence spectrometer (Edinburgh Instruments) with a 450 W ozone free xenon arc lamp that covers a range of 230-1000 nm and equipped with a solid sample holder with inserts for measurement of powder samples. This arrangement allows not only keeping an approximately constant amount of sample, but also preserving the geometry for reproducible luminescence measurements.

3. RESULTS AND DISCUSSION

Figure 2 shows the XRD patterns of the Mn-doped ZnS samples with different doping levels obtained by MSR from the Zn/Mn/S mixtures. XRD patterns show that Mn-doped ZnS samples were obtained with the wurtzite structure, although the presence of a small amount of starting Zn and S, which can be eliminated by prolonging milling longer after ignition, was also observed. Note that most reports in the literature refer to doped samples with the zinc blende structure. Papers related to the wurtzite structure are less frequent, and the stabilization of this high-temperature phase is mainly correlated with the formation of special elongated morphologies [8,15,16,39-41]. However, in our case, the wurtzite phase was obtained due to the high temperatures reached during the MSR process. Wurtzite has also been observed in samples obtained by other combustion synthesis processes [20,23,24].

The careful examination of Figure 2 also evidenced a shift of the XRD peaks towards lower angle values as the Mn content increased, which was more clearly visible for samples with a higher Mn doping level. This shift was clear evidence that Mn ions were effectively incorporated into the ZnS structure during the synthesis by the MSR process. The lattice parameters determined from the Rietveld method for the wurtzite phase are shown in Table 1 and it was confirmed the trend of the unit cell volume increase

with the Mn content. The cell parameters for the sample without Mn were in agreement

with those corresponding to the 36-1450 ZnS reference pattern from ICDD.
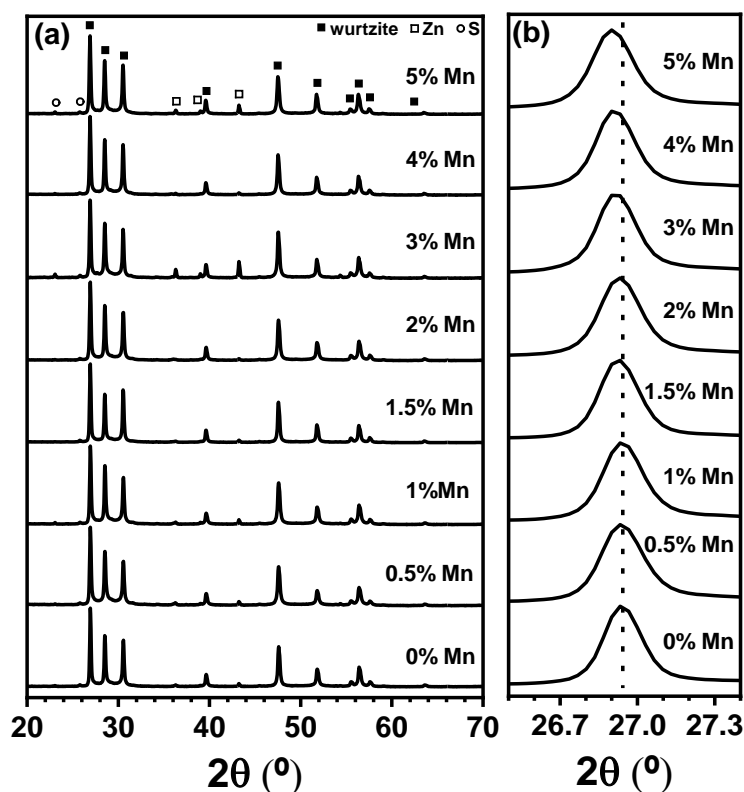

Figure 2. (a) XRD patterns of the different Zn/Mn/S mixtures after the MSR process (milling time = t_{ig} + 10 min) that show the formation of Mn-doped ZnS samples. (b) XRD patterns of the same samples in the 26.5°–27.4° 2θ region where the (100) reflection of the wurtzite phase is observed.

Representative microstructural results obtained for $Zn_{0.98}Mn_{0.02}S$ (2 mol%) and

$Zn_{0.95}Mn_{0.05}S$ (5 mol%) samples using TEM-related techniques are shown in Figures 3

and 4, respectively. Similar results were obtained for the complete set of samples. TEM

images show the same type of morphology in Figures 3a and 4a. The ring-ED patterns

(Figures 3b and 4b) obtained in both samples were the evidence of a nanocrystalline

character and indicated that the particles observed by TEM, which are forming

agglomerates, are in fact constituted by nanocrystalline domains, as evidenced in the

HRTEM micrographs (Figures 3c and 4c). Such crystalline nanodomains present a size

between 5 and 20 nm; note in Figure 3c that in the HRTEM micrograph with dimension

of 20 x 20 nm, at least 4 nanodomains with different orientations can be observed.

8

However, in the HRTEM image presented in Figure 4c with similar dimensions (20 x 20 nm), only one nanocrystallite was found. The (h, k, l) planes corresponding to the rings (marked in the EDP, Figures 3b and 4b) were indexed and belong to the wurtzite structure (hexagonal *2H*, space group P63mc). Two oriented nanodomains along the $[0\ 0\ 1]_{2H}$ and
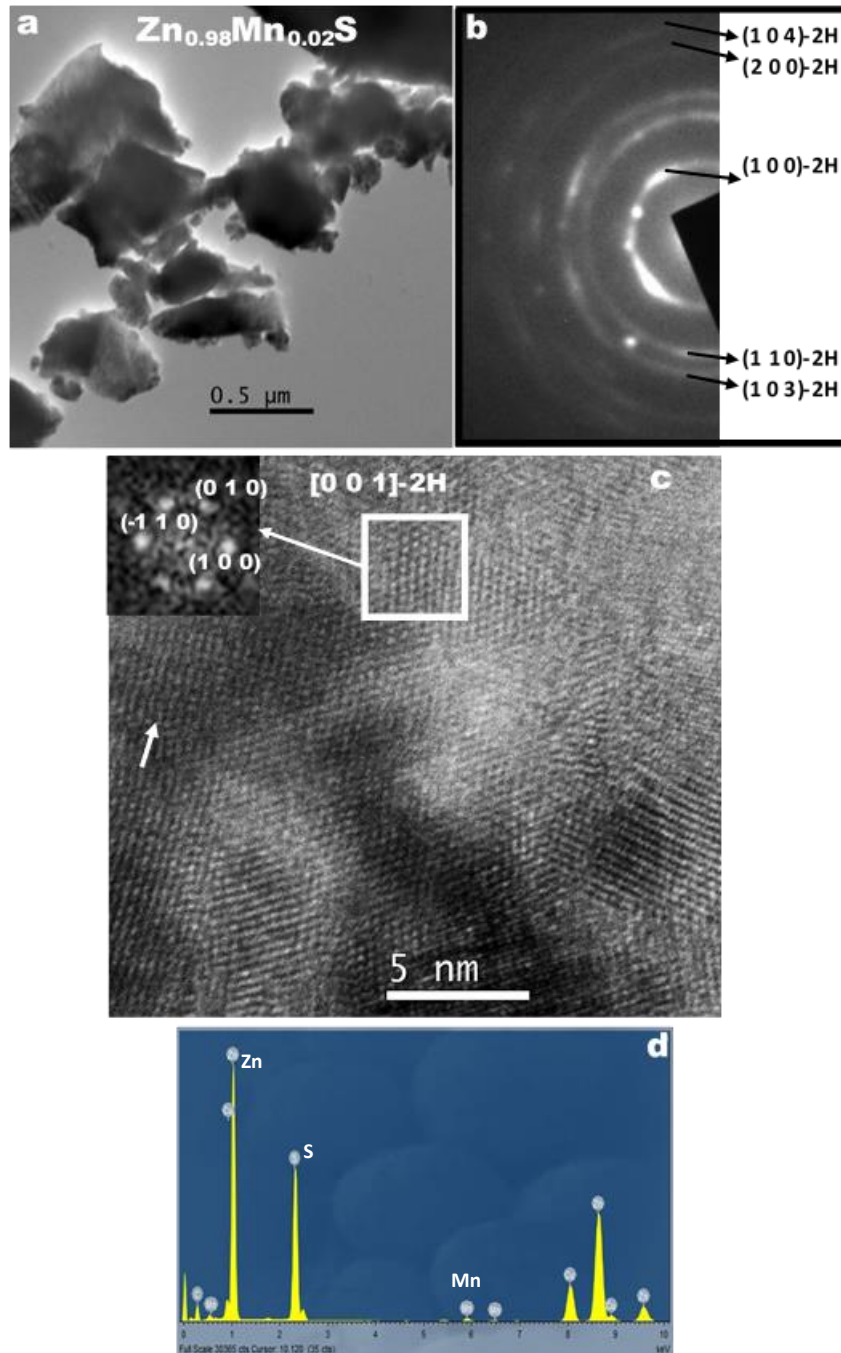

Figure 3. Microstructural characterization (TEM, EDP, HRTEM and EDX) of $Zn_{0.98}Mn_{0.02}S$ sample (2 mol%) obtained by MSR. A small nanodomain oriented along the $[0\ 0\ 1]_{2H}$ zone axis is white marked and the corresponding FFT and simulated EDP are inset in the HRTEM image.
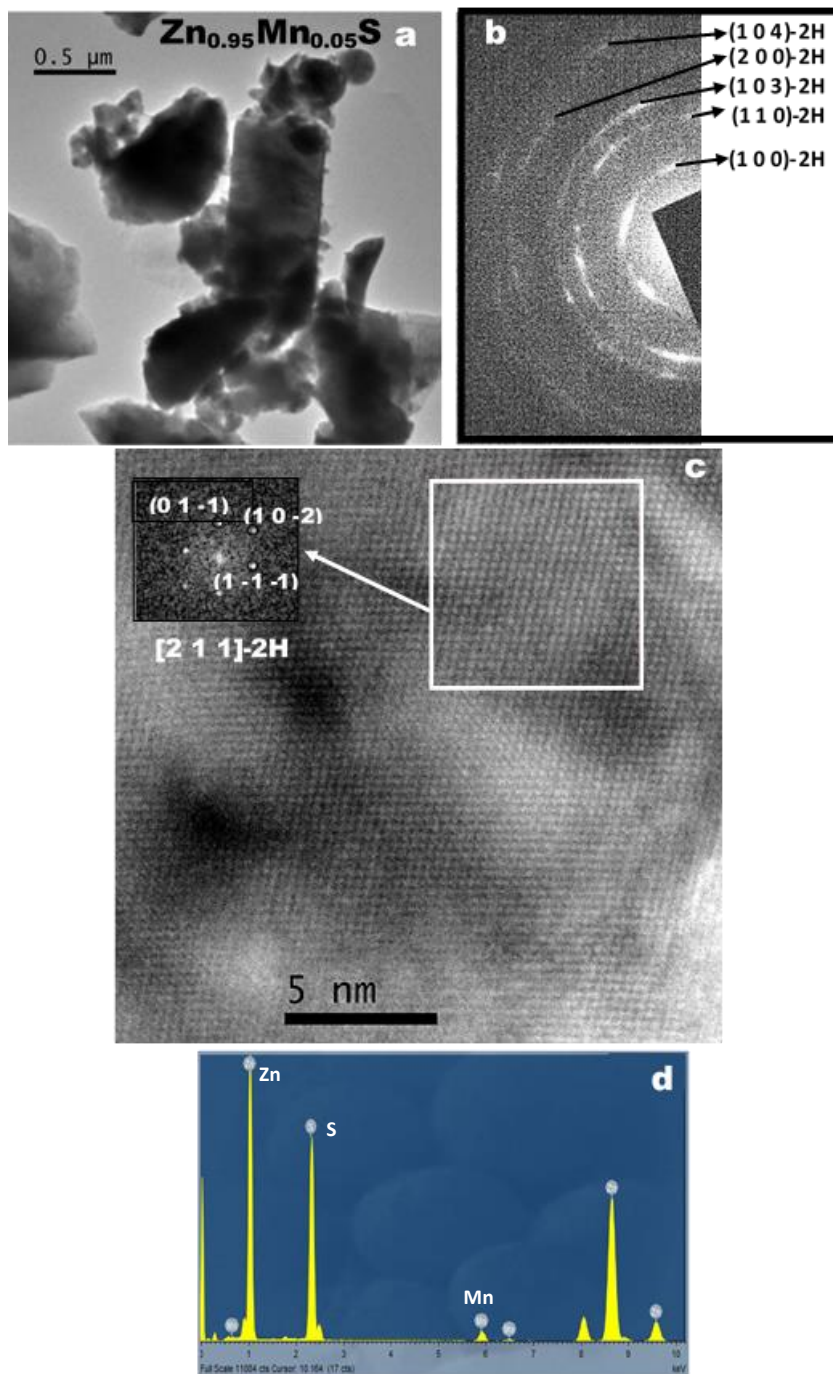
Figure 4. Microstructural characterization (TEM, EDP, HRTEM and EDX) of $Zn_{0.95}Mn_{0.05}S$ sample (5 mol%) obtained by MSR. A small nanodomain oriented along the $[2\ 1\ 1]_{2H}$ zone axis is white marked and the corresponding FFT and simulated EDP are inset in the HRTEM image.

$[2\ 1\ 1]_{2H}$ zone axes (white marked in Figures 3c and 4c) and their corresponding FFT are presented as insets in the HRTEM micrographs (Figures 3c and 4c). Some stacking faults are observed in Figure 3c (marked with a white arrow), which can be generated due to the rapid crystal growth characterizing combustion processes. Although most of the

oriented nanodomains found belonged to the wurtzite structure, few nanodomains with the zinc blende structure (cubic, space group F-43m) were also observed.

The chemical analysis of the samples was carried out by semiquantitative EDX measurements. Representative spectra of $Zn_{0.98}Mn_{0.02}S$ (2 mol%) and $Zn_{0.95}Mn_{0.05}S$ (5 mol%) samples are depicted in Figures 3d and 4d, respectively, where the presence of Mn, Zn and S is confirmed. The average values obtained for the Mn content in different areas of samples are included in Table 1. Considering the semiquantitative nature of EDX analysis, a good agreement between the nominal and final doping contents was observed, which contrasts with the larger differences normally observed in other solution-based synthetic routes [17,18]. However, a large standard deviation was obtained, suggesting some chemical heterogeneity between the particles.

TABLE 1. Lattice parameters of the wurtzite structure, the nominal and calculated by EDX Mn doping level and band gap energy (E_g) of the Mn-doped ZnS samples obtained by MSR.

nominal Mn doping (mol%)	lattice parameters			Mn doping by EDX (mol%)	E_g (eV)
	a (Å)	c (Å)	volume (Å^3)		
0	3.8176	6.2503	78.89	0	3.77
0.5	3.8195	6.2522	78.99	0.84±0.34	3.83
1	3.8191	6.2520	78.97	1.30±0.28	3.81
1.5	3.8199	6.2534	79.02	1.41±0.52	3.78
2	3.8196	6.2526	79.00	1.84±0.62	3.82
3	3.8211	6.2540	79.08	3.12±1.24	3.82
4	3.8229	6.2565	79.19	3.42±1.34	3.78
5	3.8243	6.2584	79.27	5.74±2.78	3.79

Figure 5 displays the Raman spectra in the 100-400 cm^{-1} range of samples with nominal dopant levels of 0, 2 and 5 mol%. The Raman spectrum of the ZnS sample is characteristic of the wurtzite structure and similar to others reported in the literature for this same structure [42,43]. It is dominated by strong first-order unresolved longitudinal

optical (LO) modes (A_1 and E_1 symmetry) located at ~ 343 cm^{-1}, although broad features in the 125-250 cm^{-1} range are also observed, which are associated with different second-order acoustic modes [44,45]. The absence of the transverse optical (TO) modes around 280 cm^{-1} is due to the use of a red laser excitation line and it is the result of destructive interference phenomena [43]. The strong LO mode and the absence of surface optical (SO) modes observed for the undoped ZnS sample confirm a good crystalline quality. In Mn-doped samples, new bands that grow with the Mn content are observed in Figure 5 (marked with arrows). It has already been reported that when Mn is substituted for Zn within the ZnS lattice, even at low concentration, three additional Raman bands appear between the TO and LO modes of ZnS [46,47]. Therefore, Raman characterization also confirms the effective doping of Mn in ZnS through the MSR process.
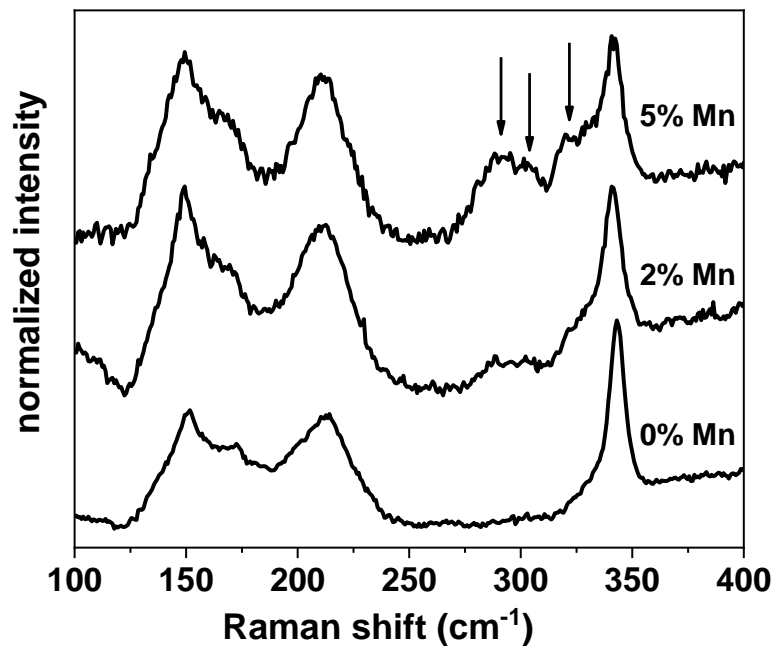

Figure 5. Raman spectra of the Mn-doped ZnS samples obtained by MSR from different Zn/Mn/S mixtures.

Figure 6 shows the DRS spectra of the different Mn-doped ZnS samples in the 200-800 nm range. The differences between the spectra are small, since the Mn content in all the samples was low (a doping level) and the DRS spectra are dominated by the

behavior of the ZnS host. The E_g values determined for the different samples were similar, within a narrow energy range of 3.77-3.83 eV, which agree with the expected value for ZnS with wurtzite structure [48]. However, noticeable differences were found when the photoluminescence properties are considered.
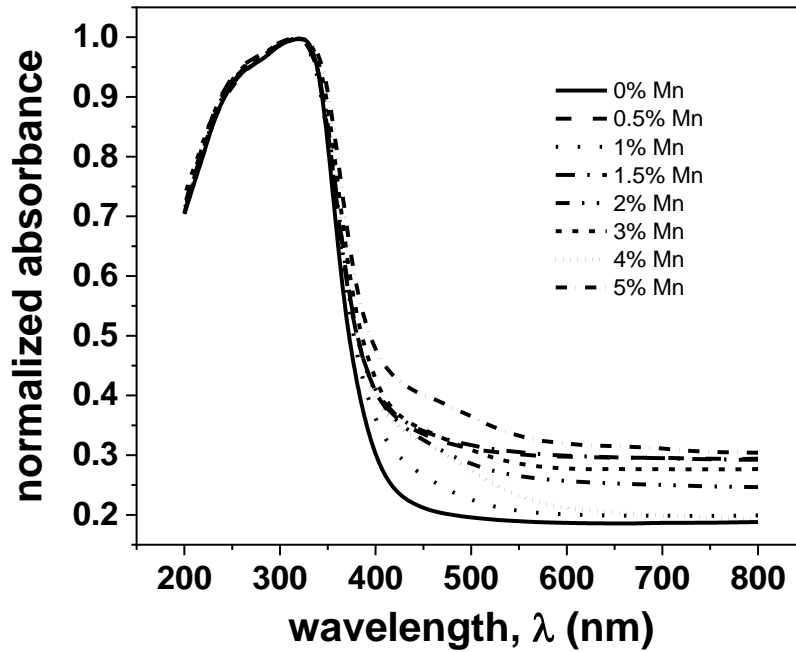

Figure 6. DRS spectra of the Mn-doped ZnS samples obtained by MSR from different Zn/Mn/S mixtures.

Figure 7 shows the PL spectra of the Mn-doped ZnS samples recorded at the excitation wavelength of 337 nm, in which an intense emission at 587 nm corresponding to the Mn^{2+} $^4T_1$-$^6A_1$ d-d transition is observed. The Mn^{2+} emission clearly dominates the different spectra, which show practically no contribution from the ZnS host. In the undoped sample, only the characteristic ZnS emission, with a significantly lower intensity, was observed. Note that this emission is red-shifted (lower energy) with respect to the theoretical band gap emission. The broad asymmetric emission band of the undoped sample, which can be decomposed at least into three contributions at ~ 416, 437 and 465 nm, is the result of the presence of different excited surface and defect states in the sample [1,49]. Figure 8 shows the PLE spectra of the Mn-doped ZnS samples monitored at 587

nm, which is characterized by the presence of a strong peak at ~ 349 nm that corresponds to the excitation of the ZnS host. The presence of the Mn emission in the doped samples, its induction through the ZnS host excitation and its high intensity with respect to the ZnS emission, which is practically suppressed, confirmed that Mn was successfully incorporated into the ZnS wurtzite structure (Mn^{2+} substitutes for Zn^{2+}) during the MSR process, facilitating an efficient energy transfer from the excited ZnS host to the Mn electronic *d* levels.
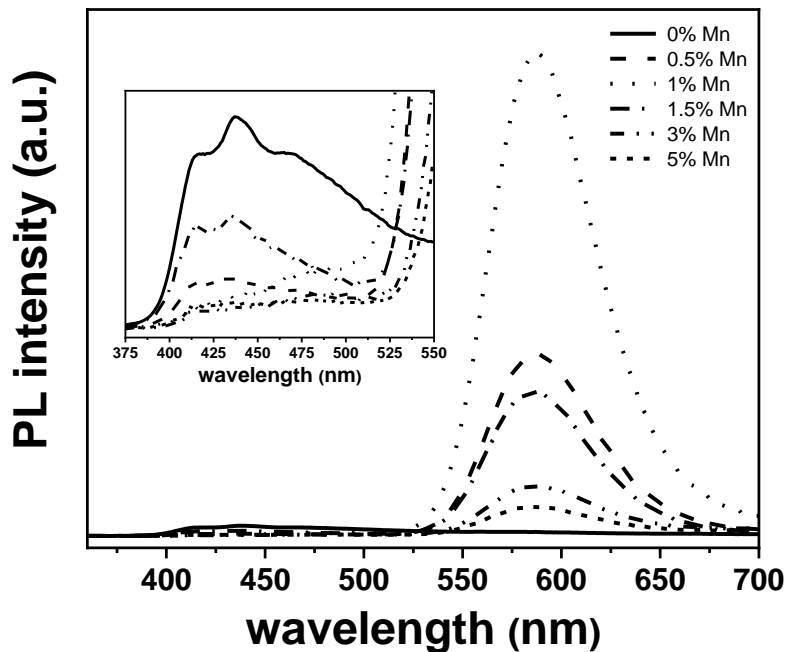

Figure 7. PL emission spectra of the Mn-doped ZnS samples obtained by MSR measured under the excitation wavelength of 337 nm.

Moreover, Figure 7 also shows a strong dependence of PL intensity on the dopant content. The maximum PL intensity at 587 nm was reached for a nominal dopant level of 1 mol%, from which a decrease in the luminescence efficiency was observed by increasing the Mn content. This optimum Mn content must be the maximum concentration that allows the presence of a major amount of isolated Mn^{2+} ions in the host structure, since the efficiency is lost due to concentration quenching as a consequence of Mn-Mn interactions between neighboring Mn ions [50]. This optimum doping level found

is in agreement with other works dealing with samples obtained by solution chemical routes and in which the actual doping level was determined by analytical techniques [17,18]. Note that in our case the Mn-doped ZnS samples present the wurtzite structure, but any difference was observed with respect to results found in the literature for doped samples with the zinc blende structure.
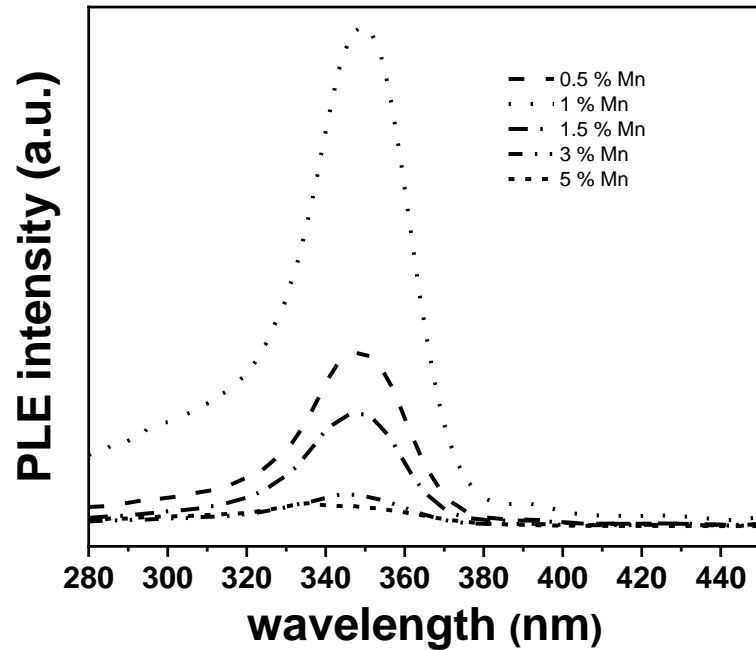

Figure 8. PLE excitation spectra of the Mn-doped ZnS samples obtained by MSR recorded for the 587 nm emission band.

The results found in the bibliography on Mn-doped ZnS obtained by combustion synthesis processes were somewhat contradictory when compared with our results. In [19], the characteristic Mn^{2+} emission was not observed, probably due to the high doping level employed (30 and 50 mol%). However, this emission was observed in [20,23], although the synthesis method only could incorporate 1 wt.% of Mn^{2+} into the ZnS crystal lattice, despite using a larger Mn content in the reaction mixture. In [22], the maximum intensity of the photoluminescence at ~ 585 nm was observed in specimens with Mn contents of 0.5 mol%. Finally, in [24], Mn-doped ZnS samples with a nominal Mn content of 1 wt.% were obtained, which presented the Mn^{2+} emission, but the PL spectra showed

a non-negligible contribution of the ZnS host, probably because the actual Mn content incorporated into the ZnS structure was lower.

On the other hand, optimal Mn contents greater than 1 mol% have been reported in doped samples obtained by solid-state synthesis methods. For example, in Mn-doped ZnS obtained by annealing a mixture of ZnS and Mn at 800ºC in a sealed vessel, a maximum luminescence was found for a 3 mol% Mn content [51]. Wang et al [52] prepared Mn-doped ZnS from ZnS and $MnCO_3$ mixtures annealed at 1100ºC and found an optimal Mn^{2+} doping concentration of 1-2 at.%. A similar optimal Mn content of 3 mol% has been reported for Mn-doped ZnS obtained from ZnS and MnO mixtures at 1100ºC [53]. However, Wang et al [54], in Mn-doped ZnS synthesized from zinc acetate, manganese acetate and thioacetamide mixtures annealed at low temperature (100-300ºC), observed no quenching phenomena and an emission intensity that increased proportionally with the doping concentration in the 1-5% range studied.

Finally, if the results of the present work are compared with those of other works dealing with milling processes, important differences were also found. For example, in [35,36], the PL measurements performed in Mn-doped ZnS samples obtained by milling Zn, Mn and S did not evidence the characteristic emission at ~ 580 nm, which infers that the samples were not properly doped. In [37], any luminescence measurement was shown and in [38], the comminution of commercial microsized $ZnS:Mn^{2+}$ samples induced only a slight improvement in PL spectra.

4. CONCLUSIONS

The ability of the mechanically-induced self-sustaining reaction (MSR) process to obtain Mn-doped ZnS samples was demonstrated. This synthetic method, which is simple

and allows the scaling up, permits an adequate control of the Mn doping level by adjusting the starting Zn/Mn/S atomic ratio of the elemental mixture subjected to milling. A wurtzite structure was obtained as a result of the high exothermic character of the formation reaction that induced a combustion process. The microstructural characterization showed that wurtzite particles were composed of misoriented nanocrystalline domains. The band gap of doped samples was practically constant in the range 3.77-3.83 eV, independently of Mn content. Photoluminescence measurements showed the characteristic 587 nm emission corresponding to the Mn^{2+} $^4T_1$-$^6A_1$ d-d transition. A strong dependence of the intensity of this emission on the doping level was found. The maximum emission was observed for a nominal doping level of 1 mol%, from which a quenching phenomenon was observed. The fact that the Mn emission was effectively induced through the ZnS host excitation and the suppression of the host emission confirmed that Mn^{2+} substitutes for Zn^{2+} in the wurtzite structure. The effective Mn doping was also confirmed by Raman spectroscopy.

Conflicts of interest

There are no conflicts to declare

BIBLIOGRAPHY.

1. N. Pradhan and D. D. Sarma, Advances in light-emitting doped semiconductor nanocrystals, J. Phys. Chem. Lett. 21 (2011) 2818–2826.

2. Y. Gong and Z. Fan, Highly selective manganese-doped zinc sulfide quantum dots based label free phosphorescent sensor for phosphopeptides in presence of zirconium (IV), Biosens. Bioelectron. 66 (2015) 533–538.

3. P. Deng, L. Q. Lu, T. Tan, Y. Jin, X. Z. Fan, W. C. Cao and X. K. Tian, Novel phosphorescent Mn-doped ZnS quantum dots as a probe for the detection of L-tyrosine in human urine, Anal. Methods 9 (2017) 287–293.

4. Z. Zhang, J. She, H. Chen, S. Deng and N. Xu, Laser-induced doping and fine patterning of massively prepared luminescent ZnS nanospheres, J. Mater. Chem. C 1 (2013) 4970–4978.

5. S. Horoz, Q. Dai, F. S. Maloney, B. Yakami, J. M. Pikal, X. Zhang, J. Wang, W. Wang and J. Tang, Absorption Induced by Mn Doping of ZnS for Improved Sensitized Quantum-Dot Solar Cells, Phys. Rev. Applied 3 (2015) 024011.

6. S. Sapra, A. Prakash, A. Ghangrekar, N. Periasamy and D. D. Sarma, Emission properties of manganese-doped ZnS nanocrystals, J. Phys. Chem. B 109 (2005) 1663–1668.

7. M. Tanaka, Photoluminescence properties of Mn^{2+}-doped II–VI semiconductor nanocrystals, J. Lumin. 100 (2002) 163–173.

8. M. Wei, J. Yang, Y. Yan, L. Yang, J. Cao, H. Fu, B. Wang and L. Fan, Influence of Mn ions concentration on optical and magnetic properties of Mn-doped ZnS nanowires, Physica E 52 (2013) 144–149.

9. E. Sotelo-Gonzalez, L. Roces, S. Garcia-Granda, M. T. Fernandez-Arguelles, J. M. Costa-Fernandez and A. Sanz-Medel, Influence of Mn^{2+} concentration on Mn^{2+}-

doped ZnS quantum dot synthesis: evaluation of the structural and photoluminescent properties, Nanoscale 5 (2013) 9156–9161.

10. C. Song, B. Chen, Y. Chen, Y. Wu, Z. Zhuang, X. Lu, X. Qiao and X. Fan, Microstructures and luminescence behaviors of Mn^{2+} doped ZnS nanoparticle clusters with different core/shell assembled orders, J. Alloys Compd. 590 (2014) 546–552

11. R. Viswanath, H. S. B. Naik, G. S. Y. Kumar, P. N. P. Kumar, G. A. Kumar and R. Praveen, EDTA-assisted hydrothermal synthesis, characterization and photoluminescent properties of Mn^{2+}-doped ZnS, J. Lumin. 153 (2014) 446–452.

12. N. T. Tuan, D. Q. Trung, N. V. Quang, N. D. Hung, N. T. Khoi, P. T. Huy, P. F. Smete, K. W. Meert and Dirk Poelman, Excitation energy dependence of the life time of orange emission from Mn-doped ZnS nanocrystals, J. Lumin. 199 (2018) 39–44.

13. B. B. Srivastava, S. Jana, N. S. Karan, S. Paria, N. R. Jana, D. D. Sarma and N. Pradhan, Highly luminescent Mn-doped ZnS nanocrystals: Gram-scale synthesis, J. Phys. Chem. Lett. 1 (2010) 1454–1458.

14. R. M. K. Whiffen, D. J. Jovanović, Ž. Antić, B. Bártová, D. Milivojević, M. D. Dramićanin and M. G. Brik, Structural, optical and crystal field analyses of undoped and Mn^{2+}-doped ZnS nanoparticles synthesized via reverse micelle route, J. Lumin. 146 (2014) 133–140.

15. M. A. Kamran, A. Majid, T. Alharbi, M. W. Iqbal, M. W. Amjad, G. Nabi, S. Zou and B. Zou, Large tunable luminescence by Mn(II) aggregates in Mn-doped ZnS nanobelts, *J. Mater. Chem. C*, 2017, **5**, 8749–8757.

16. J. Li, K. Liu, X. Zhu, M. Meng, W. Qin, Q. Liu and C. Xu, Competitive mechanism of electron transition in Mn-doped ZnS nanoribbons, J. Alloys Compd. 658 (2016) 616–620.

17. A. A. Bol and A. Meijerink, Luminescence Quantum Efficiency of Nanocrystalline ZnS:Mn^{2+}. 1. Surface Passivation and Mn^{2+} Concentration, J. Phys. Chem. B 105 (2001) 10197–10202.

18. W. Q. Peng, S. C. Qu, G. W. Cong, X. Q. Zhang and Z.G. Wang, Optical and magnetic properties of ZnS nanoparticles doped with Mn^{2+}, J. Cryst. Growth 282 (2005) 179–185.

19. D. K. Manimegalai, A. Manikandan, S. Moortheswaran and·S. A. Antony, Magneto-optical and photocatalytic properties of magnetically recyclable Mn$_x$Zn$_{1-x}$S (x = 0.0, 0.3, and 0.5) nanocatalysts, J. Supercond. Nov. Magn. 28 (2015) 2755–2766.

20. C. W. Won, H. H.Nersisyan, H. I. Won, D. Y. Jeon and J. Y. Han, Combustion synthesis and photoluminescence of ZnS:Mn^{+2} particles, J. Lumin. 130 (2010) 1026–1031.

21. H. Tanaka, E. Miyazaki and O. Odawara, Combustion synthesis of zinc-manganese-sulfur compound systems, Int. J. Self Propag. High Temp. Synth. 13 (2004) 227–232.

22. S. V. Kozitsky and A. P. Chebanenko, Electroluminescence of Mn-doped ZnS obtained by the SHS method, J. Appl. Spectrosc. 60 (1994) 338–340.

23. C. W. Won, H. H. Nersisyan, H. I. Won, D. Y. Jeon and A. G. Kirakosyan, Synthesis of ZnS Phosphor Particles in Exothermic Frontal Waves, Combust. Sci. Technol. 183 (2011) 915–927.

24. Y. Y. Bacherikov, N. P. Baran, I. P. Vorona, A. V. Gilchuk, A. G. Zhuk,·Y. O. Polishchuk, S. R. Lavorik, V. P. Kladko, S. V. Kozitskii, E. F. Venger and·N. E. Korsunska, Structural and optical properties of ZnS:Mn micro-powders, synthesized from the charge with a different Zn/S ratio, J. Mater. Sci.: Mater. Electron. 28 (2017) 8569–8578.

25. A. S. Mukasyan, A. S. Rogachev, S. T. R. Aruna, Combustion synthesis in nanostructured reactive systems, Adv. Powder Technol. 26 (2015) 954–976.

26. A. Varma, A. S. Mukasyan, A. S. Rogachev and K. V. Manukyan, Solution Combustion Synthesis of Nanoscale Materials, Chem. Rev. 116 (2016) 14493−14586.

27. E. A. Levashov, A. S. Mukasyan, A. S. Rogachev and D. V. Shtansky, Self-propagating high-temperature synthesis of advanced materials and coatings, Int. Mater. Rev. 62 (2017) 203–239.

28. M. Binnewies and E. Milke, Thermochemical Data of Elements and Compounds; Wiley VCH: Weinheim, Germany, 1999.

29. Z. A. Munir and U. Anselmi-Tamburini, Self-propagating exothermic reactions: The synthesis of high-temperature materials by combustion, Mater. Sci. Rep. 3 (1989) 277–365.

30. L. Takacs, Self-sustaining reactions induced by ball milling, Prog. Mat. Sci. 47 (20002) 355–414.

31. C. G. Tschakarov, G. G. Gospodinov and Z. Bontschev, Uber den Mechanismus der mechanochemischen Synthese anorganischer Verbindungen. J. Solid State Chem., 41 (1982) 244−252.

32. C. Chakurov, V. Rusanov, and J. Koichev, The effect of inert additives on the explosive mechanochemical synthesis of some metal chalcogenides. J. Solid State Chem. 71 (1987) 522−529.

33. A. Bakhshai, V. Soika, M. A. Susol and L. Takacs, Mechanochemical reactions in the Sn-Zn-S system: Further studies. J. Solid State Chem. 153 (2000) 371−380.

34. M. A. Avilés, J. M. Córdoba, M. J. Sayagués and F. J. Gotor, Tailoring the Band Gap in the ZnS/ZnSe System: Solid Solutions by a Mechanically Induced Self-Sustaining Reaction, Inorg. Chem. 58 (2019) 2565−2575.

35. A. Dhara, S. Sain, S. Das and S. K. Pradhan, Microstructure, optical and electrical characterizations of Mn doped ZnS nanocrystals synthesized by mechanical alloying, Mat. Res. Bull. 97 (2018) 169–175.

36. S. Sain, A. Kar, M. Mukherjee, D. Das and S. K. Pradhan, Structure, optical and magnetic characterizations of Mn doped ZnS dilute magnetic semiconductor synthesized by mechanical alloying, Adv. Powder Technol. 27 (2016) 1790–1799.

37. J. V. Tolia, M. Chakraborty and Z. V. P. Murthy, Photocatalytic degradation of malachite green dye using doped and undoped ZnS nanoparticles, Pol. J. Chem. Tech. 14 (2012) 16–21.

38. S. Hamaguchi, S. Ishizaki and M. Kobayashi, Preparation of ZnS:Mn^{2+} and other sulpher compound nanoparticles by using a ball-milling method, J. Korean Phys. Soc., 53 (2008) 3029–3032.

39. X. Wang, Q. Zhang, B. Zou, A. Lei and P. Ren, Synthesis of Mn-doped ZnS architectures in ternary solution and their optical properties, Appl. Surf. Sci. 257 (2011) 10898– 10902.

40. J. Cao, D. Han, B. Wang, L. Fan, H. Fu, M. Wei, B. Feng, X. Liu and J. Yang, Low temperature synthesis, photoluminescence, magnetic properties of the transition metal doped wurtzite ZnS nanowires, J. Solid State Chem. 200 (2013) 317–322.

41. Y. Tian, Y. Zhao, H. Tang, W. Zhou, L. Wang and J. Zhang, Synthesis of ZnS ultrathin nanowires and photoluminescence with Mn^{2+} doping, Mater. Lett. 148 (2015) 151–154.

42. Q. Xiong, J. Wang, O. Reese, L. C. L.Y. Voon and P. C. Eklund, Raman Scattering from Surface Phonons in Rectangular Cross-sectional w-ZnS Nanowires, Nano Lett. 4 (2004) 1991–1996.

43. J. H. Kim, H. Rho, J. Kim, Y. J. Choi and J. G. Park, Raman spectroscopy of ZnS nanostructures, J. Raman Spectrosc. 43 (2012) 906–910.

44. Y. C. Cheng, C. Q. Jin, F. Gao, X. L. Wu, W. Zhong, S. H. Li, and P. K. Chu, Raman scattering study of zinc blende and wurtzite ZnS, J. Appl. Phys. 106 (2009) 123505.

45. J. Serrano, A. Cantarero, M. Cardona, N. Garro, R. Lauck, R. E. Tallman, T. M. Ritter and B. A. Weinstein, Raman scattering in β-ZnS, Phys. Rev. B 69 (2004) 014301.

46. S. Jiménez-Sandoval, A. López-Rivera and J. C. Irwin, Influence of reduced mass differences on the Raman spectra of ternary mixed compounds: $Zn_{1-x}Fe_xS$ and $Zn_{1-x}Mn_xS$, Phys. Rev. B 68 (2003) 054303.

47. J. Wu, H. R. Gutierrezand P. C. Eklund, Synthesis and Raman Scattering from $Zn_{1-x}Mn_xS$ Diluted Magnetic Semiconductor Nanowires, J. Nanosci. Nanotechnol. 8 (2008) 393–399.

48. T. Trindade, P. O'Brien and N. L. Pickett, Nanocrystalline Semiconductors: Synthesis, Properties, and Perspectives, Chem. Mater. 13 (2001) 3843–3858.

49. R. Kripal, A. K. Gupta, S. K. Mishra, R. K. Srivastava, A. C. Pandey and S. G. Prakash, Photoluminescence and photoconductivity of $ZnS:Mn^{2+}$ nanoparticles synthesized via co-precipitation method, Spectrochim. Acta A 76 (2010) 523–530.

50. A. Nag, S. Chakraborty and D. D. Sarma, To dope Mn^{2+} in a semiconducting nanocrystal, J. Am. Chem. Soc. 130 (2008) 10605–10611.

51. B. J. Park, W. B. Im, W. J. Chung, H. S. Seo, J. T. Ahn and D. Y. Jeon, Internal pressure effect on cathodoluminescence enhancement of $ZnS:Mn^{2+}$ synthesized by a sealed vessel, J. Mater. Res. 22 (2007) 2838–2844.

52. X. Wang, R. Ling, Y. Zhang, M. Que, Y. Peng and C. Pan, Oxygen-assisted preparation of mechanoluminescent ZnS:Mn for dynamic pressure mapping, Nano Res. 11 (2018) 1967–1976.

53. H. Y. Lu and S. Y. Chu, The mechanism andcharacteristics of ZnS-based phosphor powders, J. Cryst. Growth 265 (2004) 476–481.

54. L. Wang, X. Xu and X. Yuan, Preparation and photoluminescent properties of doped nanoparticles of ZnS by solid-state reaction, J. Lumin. 30 (2010) 137–140.